Atmospheric stability-dependent infinite wind-farm models and the wake-decay coefficient

Pena Diaz, Alfredo; Rathmann, Ole Steen

Published in:
Wind Energy

Link to article, DOI:
10.1002/we.1632

Publication date:
2014

Document Version
Publisher's PDF, also known as Version of record

Wind Energy

WIND ENERGY
Wind Energ. (2013)
Published online in Wiley Online Library (wileyonlinelibrary.com). DOI: 10.1002/we.1632

RESEARCH ARTICLE

Atmospheric stability-dependent infinite wind-farm models and the wake-decay coefficient

Alfredo Peña and Ole Rathmann

DTU Wind Energy, Risø Campus, Technical University of Denmark, Roskilde, Denmark

ABSTRACT

We extend the infinite wind-farm boundary-layer (IWFBL) model of Frandsen to take into account atmospheric static stability effects. This extended model is compared with the IWFBL model of Emeis and to the Park wake model used in Wind Atlas Analysis and Application Program (WAsP), which is computed for an infinite wind farm. The models show similar behavior for the wind-speed reduction when accounting for a number of surface roughness lengths, turbine to turbine separations and wind speeds under neutral conditions. For a wide range of atmospheric stability and surface roughness length values, the extended IWFBL model of Frandsen shows a much higher wind-speed reduction dependency on atmospheric stability than on roughness length (roughness has been generally thought to have a major effect on the wind-speed reduction). We further adjust the wake-decay coefficient of the Park wake model for an infinite wind farm to match the wind-speed reduction estimated by the extended IWFBL model of Frandsen for different roughness lengths, turbine to turbine separations and atmospheric stability conditions. It is found that the WAsP-recommended values for the wake-decay coefficient of the Park wake model are (i) larger than the adjusted values for a wide range of neutral to stable atmospheric stability conditions, a number of roughness lengths and turbine separations lower than $\sim$ 10 rotor diameters and (ii) too large compared with those obtained by a semiempirical formulation (relating the ratio of the friction to the hub-height free velocity) for all types of roughness and atmospheric stability conditions.

KEYWORDS

atmospheric stability; boundary-layer model; infinite wind farm; Park wake model; wake-decay coefficient; wind-speed reduction

Correspondence

Alfredo Peña, DTU Wind Energy, Risø Campus, Technical University of Denmark, Roskilde, Denmark.
E-mail: aldi@dtu.dk

Received 13 September 2011; Revised 10 April 2013; Accepted 15 April 2013

1. INTRODUCTION

Most wind Park wake (WPW) models are able to estimate wind-speed reductions within the wind farm for a wide range of wind speeds, assuming neutral atmospheric conditions in most cases. These models, such as the Park wake model[1] implemented in the Wind Atlas Analysis and Application Program (WAsP),[2] predict well the energy yield losses due to wakes when analyzing long terms of meteorological (met) and wind-farm data. This is partly because in a long term, most atmospheric static stability conditions at wind turbine sites are generally close to neutral. According to Troen and Petersen,[3] the long-term atmospheric stability is just a little biased to the stable side over land and to the unstable side over water from the analysis of met stations over Northern Europe, which showed a higher amount of positive compared with negative surface heat fluxes at few offshore met masts, whereas for Peña and Hahmann[4] is slightly biased to the stable side over the North Sea on the basis of the analysis of the probability distribution function of stability measures.

When analyzing wind-farm and met data from the Horns Rev I wind farm in the Danish North Sea, Jensen[5] estimated that the annual mean array efficiency reduces from 91.5% under unstable to 85.3% under stable atmospheric conditions. Barthelmie and Jensen[6] also estimated wind-farm efficiency reductions in stable compared with unstable atmospheric conditions up to $\sim$ 9% for the wind-speed range 9–10 m s^{-1} for the Nysted wind farm in the Danish Baltic Sea. Since wind-farm operators do not want to know the annual energy production of the wind farm only but would also like to forecast the wind-farm energy output for a given set of met conditions, which can rapidly change as shown in Vincent *et al.*,[7] we need to run the WPW models for different met conditions, which include the state of the atmosphere.

Inclusion of the atmospheric stability dependency in the WPW models is not straightforward. Therefore, an alternative is to simply adjust the parameters in the models to match the observed/measured data. Barthelmie and Jensen[6] found better agreement when comparing the Park wake model with the Nysted wind-farm data by using a lower wake-decay coefficient (0.03) than that recommended in WAsP for offshore conditions (0.05). Interestingly, the amount of stable atmospheric conditions are relatively large at Nysted[6] compared with those in the North Sea,[8] implying that the more stable the atmosphere, the lower the wake-decay coefficient for the Park wake model.

In this paper, we adjust the wake-decay coefficient of the Park wake model, evaluated for an infinite array of wind turbines, to match the wind-speed reduction estimated by the infinite wind-farm boundary-layer (IWFBL) model of Frandsen.[9] The adjustment can be carried out for different wind speeds, turbine to turbine separations, surface roughness lengths and atmospheric stability conditions. Since Frandsen developed his model for neutral conditions only, we extend it for diabatic atmospheric conditions (assuming horizontal and vertical homogeneity of stability) by using local atmospheric stability corrections to the logarithmic (log) wind profile and the resistance law constants of the geostrophic drag law. The stability corrections to the log wind profile are limited to the range of atmospheric conditions and heights where the surface-layer theory is valid. Therefore, considerations should be made, particularly under stable conditions, where the theory is limited to a few tens of meters above the surface only and where the boundary-layer height (BLH) is about the size of the turbines and therefore influences the shape of the wind profile as shown in Peña *et al*.[10] and Sathe *et al*.[8] and when the atmospheric stability changes within the wind farm.

There are other techniques to study the wind-speed reductions due to wind turbine wakes.[11] Computational fluid dynamics (CFD) methods have been extensively applied for multiple wind turbines and in the last couple of years, large eddy simulation (LES) methods have gained popularity compared with the Reynolds averaged Navier–Stokes (RANS) turbulence models. This is partly due to the extension of LESs to account for atmospheric stability conditions other than neutral, which allows LES results to be compared with benchmark cases.[12] The LES technique has also been used to study large arrays of wind farms,[12–14] which can also provide the information needed to adjust the wake-decay coefficient of the Park wake model. However, RANS/LES-based wake models are about 6–7 orders of magnitude slower than the WPW or IWFBL models.

In the description of the model by Frandsen and its extension, we compare it with the results for the wind-speed reduction of an infinite array of turbines of the IWFBL model of Emeis and Frandsen (E&F)[15] and those of the Park wake model. We also show the differences between the WAsP-recommended, the semiempirical (described in Section 3) and the IWFBL-adjusted wake-decay coefficients. Results from the Park wake model are not compared with wind-farm data. Analysis of such data is as challenging as the modeling itself,[16] particularly for different atmospheric stability conditions because since most wind farms have no means to estimate stability, it is difficult to separate the effect on wind-farm power production of stability, wind speed and turbulence from real data[6] and because in large wind farms, turbines do not operate concurrently and optimally all the time.

2. IWFBL MODELS

2.1. Review

The IWFBL model of Frandsen[9] assumes that within an infinite wind farm with the same turbine type and dimensions, two layers in the atmospheric boundary layer (ABL) are distinguished, one above and one below the turbines' hub height h as shown in Figure 1. At h, the shear of both layers is linked as

$$\rho \boldsymbol{u}_{*2}^2 = \rho \boldsymbol{u}_{*1}^2 + t, \tag{1}$$

where $\boldsymbol{u}_{*2}$ and $\boldsymbol{u}_{*1}$ are the friction velocities within the above and below layers, respectively, and t is the jump in shear due to the turbines. The latter is given as $t = \rho c_t u_h^2$, ρ being the air density, u_h the hub-height spatial average wind speed within the wind farm and c_t the areal homogenously distributed thrust coefficient,

$$c_t = \frac{\pi}{8} \frac{C_t}{s_r s_f}, \tag{2}$$

where $s_r = x/D_r$ and $s_f = y/D_r$, x and y being the along-wind and cross-wind turbine to turbine distances, respectively, C_t the turbine's thrust coefficient and D_r the rotor diameter.

Since the idea is to derive an expression for u_h by using equation (1), Frandsen[9] applied the log wind profile to estimate $\boldsymbol{u}_{*1}$ and $\boldsymbol{u}_{*2}$ at hub height from the true (z_o) and the effective (z_{oo}) wind-farm roughness lengths, respectively.

$$\boldsymbol{u}_{*1} = \frac{u_h \kappa}{\ln(h/z_o)} \quad \text{and} \quad \boldsymbol{u}_{*2} = \frac{u_h \kappa}{\ln(h/z_{oo})}, \tag{3}$$

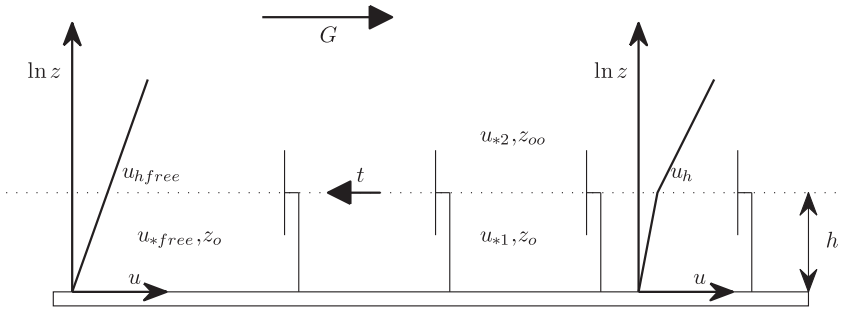

Figure 1. The infinite wind-farm boundary-layer model concept of Frandsen.[9] Upstream of the wind farm (free flow), there is one layer with the undisturbed stress scale and background roughness ($\boldsymbol{u}_{*\text{free}}$, z_o), and within the wind farm, two layers are assumed to meet at hub height h: the lowest with the background roughness and a low-stress-scale $\boldsymbol{u}_{*1}$, and the highest with the effective wind-farm roughness z_{oo} and a high-stress-scale $\boldsymbol{u}_{*2}$.

where κ is the von Kármán constant (≈ 0.4). Frandsen[9] used a corrected version of the simplified geostrophic drag law of Jensen,[17]

$$\boldsymbol{u}_* = \frac{\kappa G}{\ln\left(\frac{G}{f_p z_o}\right)}, \tag{4}$$

where G is the geostrophic wind speed and $f_p = f_c \exp(A_*)$, f_c being the Coriolis parameter and A_* a modified A parameter from the resistance-law constants, to derive an expression for the effective roughness as a function of the velocity scales:

$$z_{oo} = \frac{G}{f_p} \exp\left(\frac{-\kappa G}{\boldsymbol{u}_{*2}}\right). \tag{5}$$

Equation (5) is then used to eliminate the $\boldsymbol{u}_{*2}$ dependency on z_{oo} in equation (3, right), which results in

$$\boldsymbol{u}_{*2} = \frac{\kappa\,(G - u_h)}{\ln\left(\frac{G}{h f_p}\right)}. \tag{6}$$

For a simple derivation of u_h from equation (1), Frandsen[9] defined $K_2 = (1/\kappa)\ln[G/(h f_p)]$ and $K_1 = (1/\kappa)\ln(h/z_o)$, and thus,

$$\boldsymbol{u}_{*1} = \frac{u_h}{K_1} \quad \text{and} \quad \boldsymbol{u}_{*2} = \frac{G - u_h}{K_2}. \tag{7}$$

Substituting both forms in equation (7) into (1) leads to the solution for u_h, i.e., the IWFBL model of Frandsen where

$$u_h = \frac{G}{1 + K_2\sqrt{c_t + K_1^{-2}}}. \tag{8}$$

The wind-speed reduction R_u for the IWFBL model of Frandsen is then given as

$$R_u = \frac{1 + K_2\sqrt{K_1^{-2}}}{1 + K_2\sqrt{c_t + K_1^{-2}}}, \tag{9}$$

which is the ratio of u_h to the asymptotic overall mean wind speed at hub height, i.e., $u_h(c_t \neq 0)/u_h(c_t = 0)$. Equation (8) guarantees that $u_h(c_t = 0)$ is equal to $u_{h\text{free}}$, i.e., the undisturbed hub-height wind speed, as expected. It should be noted that by using any form of the geostrophic drag law, the ABL is assumed in this model to be barotropic and homogenous in terms of flow, atmospheric stability conditions and roughness (valid for large footprint areas).

Emeis and Frandsen[15] further developed another IWFBL model on the basis of the mixing-length theory. Shortly, they assumed the specific turbulent downward momentum flux, τ/ρ, to be driven by the vertical wind-speed gradient above the

wind farm. Using a momentum exchange coefficient K_m to parameterize this flux, E&F related it with the mixing length l as

$$\tau/\rho = K_m \frac{u_o - u_h}{\Delta z} = \frac{l^2}{\Delta z^2}(u_o - u_h)^2, \tag{10}$$

where u_o is the undisturbed wind speed at a height $z = h + \Delta z$ above the wind farm. This flux is assumed to be in balance with the momentum loss due to the turbines.

$$c_t' u_h^2 = \frac{l^2}{\Delta z^2}(u_o - u_h)^2, \tag{11}$$

where c_t' is the drag coefficient of the turbines. The surface drag coefficient is defined as $c_s = u_*^2/u_h^2$ with $\boldsymbol{u}_* = u_h\,\kappa\ln(h/z_o)^{-1}$ (so it can be shown that $c_s = K_1^{-2}$). The effective drag coefficient, $c_{t\text{eff}}$, results from the combination of that of the surface and the one from the turbines, i.e., $c_{t\text{eff}} = c_t' + c_s$.

In E&F, there are two reductions: the first is given by estimating the ratio u_h/u_o from equation 11; the second is found similarly but by replacing c_t' by $c_{t\text{eff}}$. The wind-speed reduction equivalent to equation 9 is found from the ratio of the aforementioned two reductions.

$$R_u = \frac{1 + (\Delta z/l)\sqrt{c_s}}{1 + (\Delta z/l)\sqrt{c_{t\text{eff}}}}. \tag{12}$$

Since it is straightforward to derive c_t from the thrust curve of the wind turbines in the wind farm, we assume that $c_t' = c_t$ in this study. When comparing equations (9) and (12), it can easily be demonstrated that they are identical if $\Delta z/l = K_2$. So, one of their main differences is that the IWFBL model of Frandsen depends on $u_{h\text{free}}$ through both G (via K_2) and C_t (which for a wind turbine varies with wind speed), whereas the IWFBL model of E&F, equation (12), is only dependent on $u_{h\text{free}}$ through C_t provided that l is wind-speed independent.

For neutral atmospheric conditions, E&F suggested $\Delta z/l \approx 2/\kappa$, which in terms of the IWFBL model of Frandsen means $\ln[G/(hf_p)] \approx 2$. Such approximation for a place in a rural area ($z_o = 0.025$ m) or at an offshore location ($z_o = 0.0002$ m), both assuming $h = 70$ m, $u_{h\text{free}} = 10$ m s^{-1}, $A_* = 4.53$ and latitude of 55.5°, is rather low, since $\ln[G/(hf_p)] = 3.54$ and 2.73, respectively*. Therefore, R_u is generally lower for the IWFBL model of Frandsen than that for E&F. This, as shown later, is valid for a range of wind speeds and atmospheric stability conditions.

The main 'drawbacks' of the IWFBL model of E&F are that (i) Δz is rather difficult to estimate and (ii) the mixing-length concept might be inappropriate when modeling wakes.[18] The approach by Frandsen also has drawbacks related to (i) the assumption that at some level above the hub height, the wind-farm wind speed approaches the geostrophic wind-speed value and (ii) the value of A_*, since as a modified A parameter of the geostrophic drag law, it is rather uncertain and depends on atmospheric stability among others.[19]

Figure 2 shows the wind-speed reduction comparison between the IWFBL model of Frandsen and that of E&F for different turbine to turbine separations, s, and roughness lengths†. As mentioned, the values for R_u from the IWFBL model of E&F are larger (lower reductions) than those from the approach by Frandsen, following its behavior with turbine to turbine distance. There is a faster change in wind-speed reduction with separation, and the differences (between models) are larger within the range of turbine separations where most wind farms lie, i.e., $s < 10$.

The previous comparison is based on a fixed undisturbed hub-height wind speed and thus on a fixed C_t value. When performing a similar analysis (not shown) but for a fixed turbine to turbine separation and surface roughness and different undisturbed hub-height wind speeds, which translate into a range of C_t values, we find similar wind-speed reductions for both IWFBL models, being the R_u values of the E&F model generally larger than those of Frandsen (Frandsen's reductions are only lower for very low $u_{h\text{free}}$ values). For the analysis, we chose a C_t curve from a 2 MW horizontal-axis wind turbine with a near-constant C_t within the low-wind-speed range and decreasing values with increasing wind speed.

2.2. Atmospheric stability dependency

Emeis[20] extended the IWFBL model of E&F to account for diabatic atmospheric stability conditions. Since R_u is a function of the mixing length l in equation (12), it was rather simple to extend l for diabatic conditions by using Monin–Obukhov similarity theory (MOST),[21] i.e., adding the dimensionless wind shear ϕ_m, which is a function of the stability parameter z/L, where z is the height above surface and L the Obukhov length. L is a local stability measure, which is assumed in

*G is estimated from the simplified geostrophic drag law, equation (4), and related to $u_{h\text{free}}$ through the log wind profile similar to equation (3).

†For simplicity, it is hereafter always assumed that $s_r = s_f = s$.

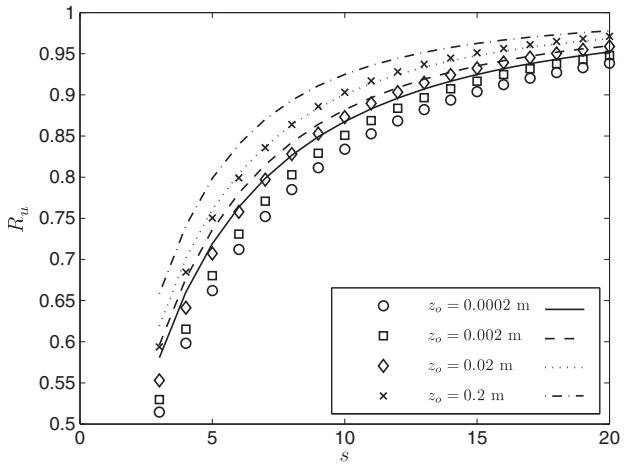

Figure 2. Wind speed reduction R_u comparison between the IWFBL models of Frandsen[9] (in markers) and E&F[15] (in lines) for different dimensionless turbine to turbine separations s and surface roughness values z_o (see legend). The models are evaluated with $C_t = 0.88$, $h = 70$ m, $u_{h\text{free}} = 10$ m s^{-1}, $z_o = 0.0002$ m, $A_* = 4.53$ and latitude of 55.5°.

MOST to be constant with height within the surface layer; in Emeis[20] and in this study, by correcting the wind shear by using a local L value, we extend its use beyond its original intend, since we further have to assume L to be constant with height above the surface layer and within the wind farm (see more details on these issues in the Section 4).

Because of the different formulations of l,[22] this extension can be carried out in several ways, and Emeis[20] tried different forms including $l = \kappa z \phi_m^{-1}$, which was proven to be valid within the surface layer when compared with turbulence measurements and spectra.[23] Since $\Delta z/l$ and K_2 are equivalents, we can also extend equations (8) and (9) by using $\phi_m(h/L)$. Further, as Emeis did it for c_s, K_1 has to be extended for stability conditions by means of the stability correction of the log wind profile ψ_m, which comes from the integration of ϕ_m, so ψ_m is also a function of z/L. u_h, for example, becomes

$$u_h = \frac{G}{1 + \phi_m(h/L) K_2 \sqrt{c_t + K_1^{-2}}}. \tag{13}$$

However, there is an inconsistency in equation (13) because u_h should equal $u_{h\text{free}}$ when $c_t = 0$. They are indeed equal under neutral conditions because $\phi_m = 1$ and $\psi_m = 0$ for $h/L = 0$. When $h/L \neq 0$, on the other hand, $u_h(c_t = 0)$ from equation (13) becomes h-dependent and does not approach the $u_{h\text{free}}$ value.

One way to avoid such 'inconsistency' is by including the stability correction function (ψ_m) to the log wind profiles within the two layers in equation (3), so that within the wind farm and at hub height,

$$\boldsymbol{u}_{*1} = \frac{u_h \kappa}{\ln(h/z_o) - \psi_m(h/L)} \tag{14}$$

and

$$\boldsymbol{u}_{*2} = \frac{u_h \kappa}{\ln(h/z_{oo}) - \psi_m(h/L)}. \tag{15}$$

In the absence of a local stability measure at hub height within the wind farm, it is assumed that L, in equations 14 and 15, is equal to a stability input given upstream the wind farm. One can work out the derivation of u_h, in a similar way as that explained in Section 2.1 (see steps between equations 4–6) and finds (by inserting z_{oo} in equation (5) into (15)).

$$\boldsymbol{u}_{*2} = \frac{\kappa(G - u_h)}{\ln\left(\frac{G}{h f_p}\right) + \psi_m(h/L)}. \tag{16}$$

Therefore, to solve u_h in equation (1), K_1 and K_2 have to be redefined as $(1/\kappa)\left[\ln(h/z_o) - \psi_m(h/L)\right]$ and $(1/\kappa)\left[\ln[G/(h f_p)] + \psi_m(h/L)\right]$, respectively. The expressions for u_h and R_u are then formally the same as those in equations (8) and (9), also valid for neutral conditions.

However, A_* (included in the modified Coriolis parameter f_p in equation 4) also depends on the state of the atmosphere, as this is close related to the resistance law constants A and B, which have been found to vary with stability. This dependency is classically described by extending A and B to be functions of the dimensionless stability parameter $\mu_o = \kappa \boldsymbol{u}_*/(f_c L)$. Despite disagreement among researchers on the forms of $A(\mu_o)$ and $B(\mu_o)$, due to the variety of data used in the different studies and their high uncertainty, it is possible to get empirical formulations for both.[24] On this basis, the dependency of A_* on atmospheric stability, $A_*(\mu_o)$, can be derived (see Appendix A for details).

For a given $u_{h\text{free}}$ value and local stability condition (an L value at a given height upstream the wind farm), G can then iteratively be estimated using the simplified geostrophic drag law, equation (4) (now including the $A_*(\mu_o)$ stability dependence) and the upstream-undisturbed friction velocity $u_{*\text{free}}$ derived from the diabatic wind profile,

$$u_{*\text{free}} = \frac{u_{h\text{free}}\,\kappa}{\ln(h/z_o) - \psi_m(h/L)}. \tag{17}$$

Now, it is important to notice that in the non-neutral cases, K_2 depends on $\boldsymbol{u}_*$ through A_*:

$$K_2(\boldsymbol{u}_*) = \frac{1}{\kappa}\left[\ln\left(\frac{G}{h f_c}\right) - A_*(\mu_o) + \psi_m(h/L)\right]. \tag{18}$$

Thus, R_u in equation (9) must be modified as

$$R_u = \frac{1 + K_2(u_{*\text{free}})\sqrt{K_1^{-2}}}{1 + K_2(u_{*2})\sqrt{c_t + K_1^{-2}}}, \tag{19}$$

where $\boldsymbol{u}_{*2}$ is found iteratively from the simplified geostrophic drag law but by using the expression for z_{oo} for non-neutral conditions (see Appendix B for its derivation).

$$z_{oo} = h \exp\left[\frac{-\kappa}{\sqrt{c_t + K_1^{-2}}} - \psi_m(h/L)\right]. \tag{20}$$

This procedure ensures that u_h, in equation (8) evaluated for $c_t = 0$, gives $u_{h\text{free}}$.

2.2.1. Model behavior

Figure 3 shows the extended IWFBL model of Frandsen for a range of dimensionless atmospheric stabilities h/L, a number of roughness lengths and a fixed dimensionless turbine to turbine distance. For the range of atmospheric stabilities, R_u always increases with high roughness length values (similar to Figure 2). The striking result is that the variation of

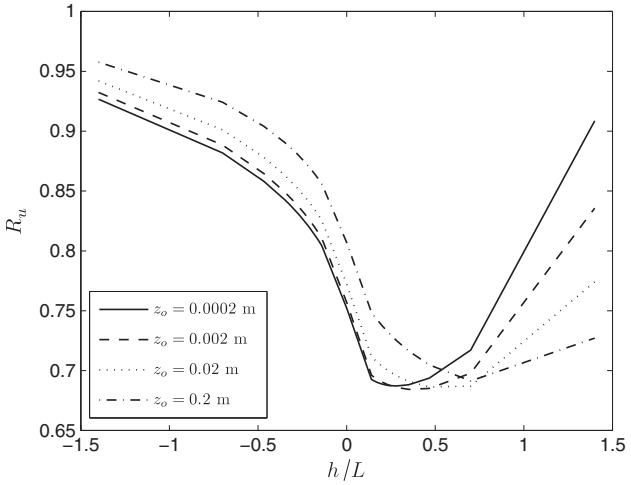

Figure 3. The wind-speed reduction R_u of the extended IWFBL model of Frandsen for a range of dimensionless atmospheric stabilities h/L, a number of surface roughness values z_o (see legend) and a fixed dimensionless turbine–turbine separation $s = 7$. The model is evaluated with $C_t = 0.88$, $h = 70$ m, $u_{h\text{free}} = 10$ m s^{-1} and latitude of 55.5°.

R_u is much higher for this broad range of atmospheric stabilities than for the rather wide range of roughness lengths, with general low-wind-speed and high-wind-speed reductions under unstable and stable atmospheric conditions, respectively.

At a given positive value of h/L (dependent on the given z_o value), R_u starts to increase with increasing stable conditions. This is because $u_{h\text{free}}$ is used as the only wind-speed input parameter to the model and for this case ($h = 70$ m), and for stable and very stable conditions, such a height is comparable to the BLH that can indeed be below 50–70 m in stable and very stable conditions. MOST (strictly valid for $\sim 10\%$ of the BLH only) then predicts a too high and unrealistic stability correction when estimating $u_{*\text{free}}$ from $u_{h\text{free}}$, which is used for computing G in a range where the stability corrections to the A and B functions and, thus, A_* in the simplified geostrophic drag law is less applicable. A way to avoid the increasing R_u values for stable conditions is by using, as an input parameter for the model, a wind speed not at hub height but at a height well inside the surface boundary layer, where MOST is well applicable.

We can also compare the results for the model of Emeis, i.e., the atmospheric stability-extended IWFBL model of E&F, and the extended IWFBL model of Frandsen for different atmospheric stability conditions and dimensionless turbine to turbine separations. This is illustrated in Figure 4 for an offshore site, where the models have the same behavior with turbine separation distances and atmospheric stability. As for the previous comparisons, the Frandsen's-type model shows larger wind-speed reductions than those from the Emeis'-type model for neutral conditions. For the computed stable and unstable conditions ($L = 100$ m and $L = -50$ m, respectively), the reductions are larger for the Emeis'-type model. This is partly due to the reference height used for the free wind speed; when using a low value for h, R_u from Emeis' model becomes higher than that of the extended model of Frandsen under stable conditions.

2.3. Wind profiles

We can also compute the spatial average wind profiles within the wind farm (by assuming L to be vertically and horizontally constant), which can be used to analyze the effect of the wind farm in the ABL (not only at hub height) and to compare with the LES results (e.g., those in Lu and Porté-Agel,[12] and Calaf *et al.*,[14]) by using similar functions as those in equations (14) and (15), first by estimating $u_{*\text{free}}$ for the different stability conditions, as in equation (17), which is then used for the estimation of G (by using a stability-corrected A_* value). z_{oo} is directly computed from equation (20). They become

$$u(z \leq h) = \frac{\boldsymbol{u}_{*1}}{\kappa}\left[\ln\left(\frac{z}{z_o}\right) - \psi_m\left(\frac{z}{L}\right)\right] \tag{21}$$

and

$$u(z \geq h) = \frac{\boldsymbol{u}_{*2}}{\kappa}\left[\ln\left(\frac{z}{z_{oo}}\right) - \psi_m\left(\frac{z}{L}\right)\right]. \tag{22}$$

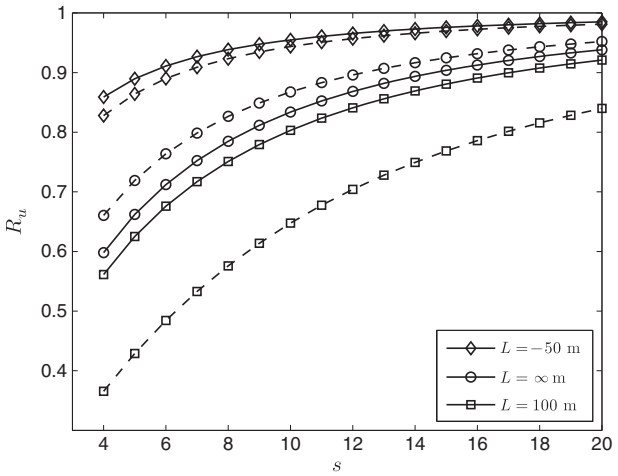

Figure 4. A comparison between the wind-speed reduction R_u of the extended IWFBL model by Frandsen (solid lines) and the model by Emeis[20] (dashed lines) for different atmospheric stabilities (see legend) and dimensionless turbine–turbine distances s. The models are evaluated with $C_t = 0.88$, $h = 70$ m, $u_{h\text{free}} = 10$ m s^{-1}, $z_o = 0.0002$ m and latitude of 55.5°.

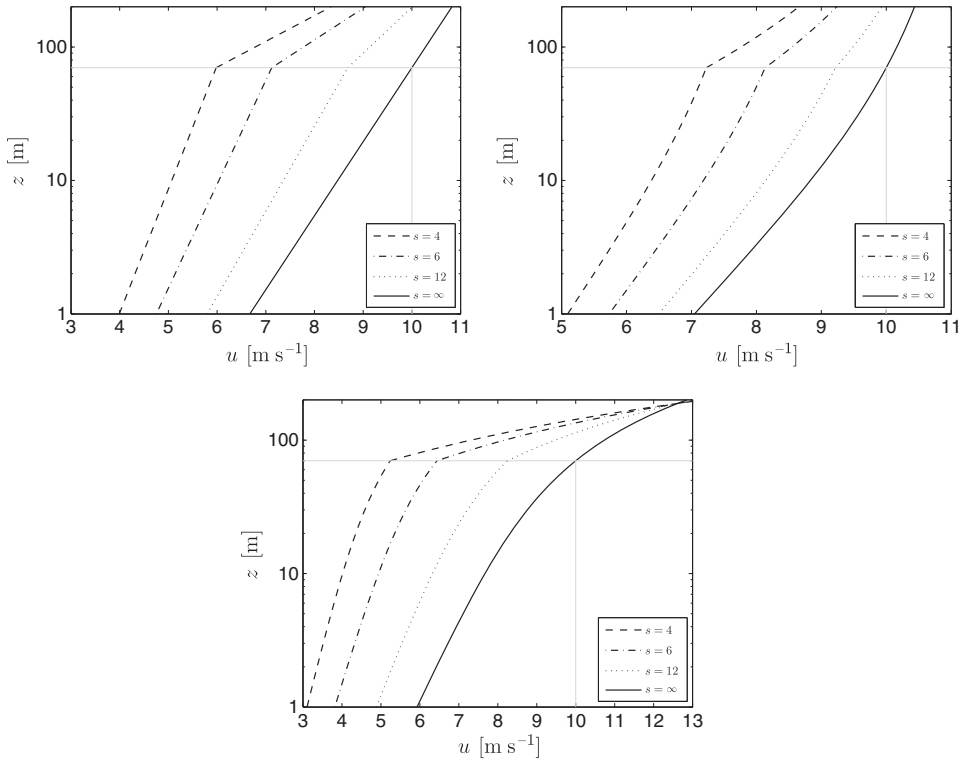

Figure 5. Variation of the spatial average wind speed u with height z for the extended IWFBL model by Frandsen within an offshore wind farm ($z_o = 0.0002$ m) for a number of dimensionless turbine–turbine separations s and atmospheric stabilities (top left—$L = \infty$ m, neutral; top right—$L = -200$ m, unstable; and bottom—$L = 200$ m, stable). In gray dotted lines are indicated the hub height ($h = 70$ m) and hub-height free wind-speed ($u_{h\text{free}} = 10$ m s^{-1}) levels. The model is evaluated with $C_t = 0.88$ and latitude of 55.5°.

Figure 5 illustrates wind profiles within an offshore wind farm for different dimensionless turbine to turbine separations and atmospheric stability conditions. Except for $s = \infty$ ($c_t = 0$), a kink in the wind profile is distinguished at hub height ($h = 70$ m), as expected. It is interesting to note that all these wind profiles are computed using $u_{h\text{free}} = 10$ m s^{-1}, which is equal to the estimation of u_h under all stability conditions and $s = \infty$.

It is important to notice that both layers (above and below h) are modeled using the approach of MOST. As h increases, e.g., with larger turbines, the above-h layer will be affected by the BLH and the baroclinicity (among others), and the MOST approach is less valid. Also, the stable corrections from MOST predict very large wind shears for the above-h layer, which lead to wind speeds $u(s \neq 0)$ above the undisturbed ones $u(s = \infty)$ already at 200 m in Figure 5-bottom.

3. INFINITE PARK WAKE MODEL

The Park wake model implemented in WAsP is based on the momentum wake model by N. O. Jensen (hereafter known as NOJ),*[25] where the wind speed immediately before the first wake-affected turbine, u_1, can be estimated as (Figure 6)

$$u_1 = u_{\text{free}}\left[1 - \frac{a}{(1 + k_w\ x/r_o)^2}\right], \tag{23}$$

where u_{free} is the upstream undisturbed wind speed, a the induction factor ($a = 1 - \sqrt{1 - C_t}$), k_w the momentum entrainment or wake-decay coefficient and r_o the initial wake radius behind the rotor. In the Park wake model, r_o is equal to the turbine's rotor radius r_r. Frandsen[9] proposed, by semiempirical means, $k_w \approx 0.5/\ln(h/z_o)$, which suggests that k_w is related to the atmospheric turbulence characteristics because $0.5/\ln(h/z_o) \approx u_{*\text{free}}/u_{h\text{free}}$ under neutral stability conditions.

*Although commonly referred to as a momentum conservation model, NOJ model conserves mass and not momentum within the control volume.

DOI: 10.1002/we

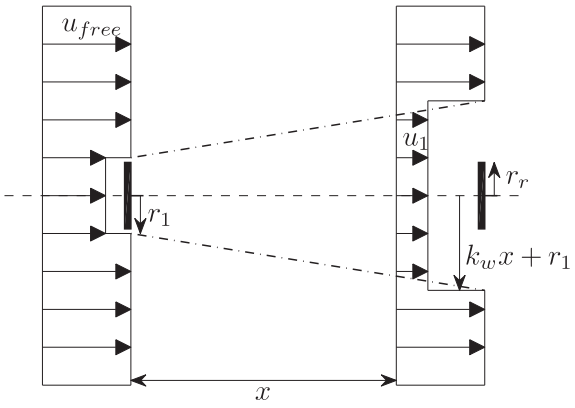

Figure 6. Momentum wake model concept by Jensen.[25] The wind speed immediately before a wake-affected turbine u_1 is estimated as a function of the distance to the upstream turbine x with rotor radius r_r, the free wind speed u_{free}, and the thrust coefficient and the wake-decay coefficient k_w.

Therefore, the wind-speed reduction in the Park wake model is also a function of k_w. The ground interaction of a wake is modeled by adding the wake reflected at the surface, i.e., a wake seemingly originating from a reflected 'underground rotor'. The surface interaction is then modeled by considering the combined effect of the direct and the reflected wakes. Further, the efficiency of the wind turbine cluster is estimated by combining the effects of four types of overlapping wakes[1]:

1. From directly upwind rotors (NOJs original approach).
2. Reflected 'underground rotors' directly upwind.
3. Shading rotors upwind but left or right to the wind direction.
4. Reflected shading 'underground rotors' upwind but left or right to the wind direction.

The combined effect of two or more overlapping wakes on a downwind rotor was modeled through an empirical quadratic summation rule.[1] Here, the partial wake overlap with a rotor is considered by applying the overlap fraction to the speed deficits of the individual wake. Thus, the rotor diameter is required as an input to the model. Rathmann *et al.*[26] analytically solved the contribution of the four types of wakes (described earlier) for an asymptotically infinite number of wind turbines. This is described here as the 'infinite Park wake model' (IPW) (Appendix C).

3.1. Adjusted wake-decay coefficient for the infinite Park wake model

When using the Park wake model, we are required of the wake-decay coefficient for the particular site. To a first approximation, it is common procedure and recommended to use $k_w = 0.050$ and $k_w = 0.075$ when performing wake analysis in WAsP over sea and land surfaces, respectively. However, k_w should be estimated for the particular z_o value and atmospheric stability condition of the site, since $k_w \approx u_{*\text{free}}/u_{h\text{free}} = \kappa/[\ln(h/z_o) - \psi_m(h/L)]$, where the correction due to atmospheric stability ψ_m is here already considered from that form proposed by Frandsen.[9] This already results in much lower k_w values than those recommended in WAsP for a wide range of roughness values and stabilities; k_w is lower for low compared with high roughness values and higher for unstable compared with stable conditions.

Figure 7 compares the wind-speed reduction from the IPW model—when using two types of k_w-values: from the form $k_w = u_{*\text{free}}/u_{h\text{free}}$, as shown earlier (so we again assume L to be invariant within the wind farm), and the WAsP-k_w values—with that from the IWFBL model by Frandsen for neutral conditions, different dimensionless turbine to turbine separations and a number of roughness lengths. The IPW model shows the same behavior as the IWFBL model, i.e., the higher the wind-speed reductions, the smoother the terrain and the shortest the turbine to turbine separation. The IPW model using the WAsP-k_w values shows similar reductions compared with the IWFBL model, slightly higher ones for offshore conditions. The IPW model using $k_w = u_{*\text{free}}/u_{h\text{free}}$ shows much higher reductions compared with the IWFBL model for all roughness lengths and similar ones to the IPW model using the WAsP-k_w value for $z_o = 0.2$ m only. This result already illustrates that the recommended WAsP-k_w values seem to be too high for wind farms located on flat and homogeneous terrain, except for areas with high roughness values such as forests.

When the IPW model is adjusted so that it gives the same wind-speed reductions as those of the IWFBL model of Frandsen, k_w has to be modified/adjusted, and thus, it becomes dependent not only on z_o (k_w increases with increasing z_o values) but also on turbine separation as shown in Figure 8. The 'adjusted' k_w values are generally much lower for smaller

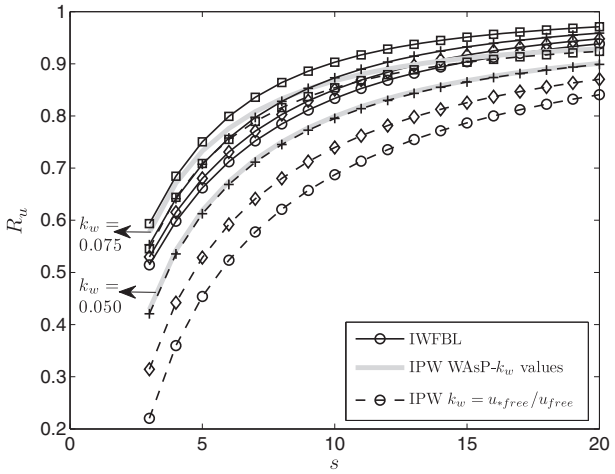

Figure 7. Comparison of the wind-speed reduction R_u between the IWFBL model of Frandsen[9] (solid lines with markers) and the IPW model for neutral conditions (by using the form $k_w = u_{*\text{free}}/u_{h\text{free}}$), a number of roughness values (∘ $z_o = 0.0002$ m, ⋄ $z_o = 0.002$ m, + $z_o = 0.02$ m and □ $z_o = 0.2$ m) and dimensionless turbine–turbine separations s. The IPW model is also evaluated with the recommended WAsP-k_w values (0.075 and 0.050 in gray solid lines). All models are evaluated with $h = 70$ m, $D_r = 80$ m, $A_* = 4.53$, $u_{h\text{free}} = 10$ m s^{-1} and latitude of 55.5°.

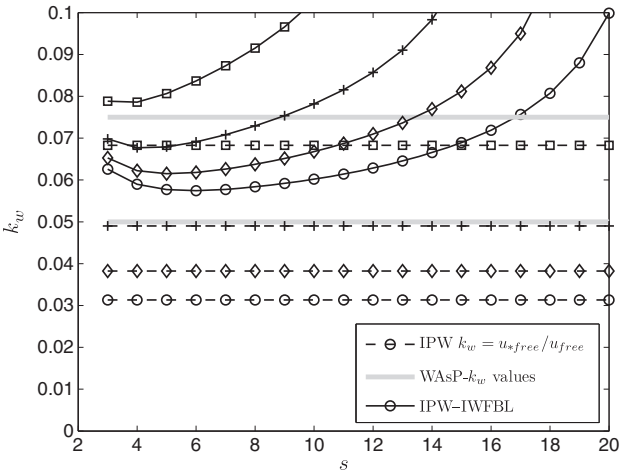

Figure 8. Variation of the wake-decay coefficient k_w (i) by assuming the form $k_w = u_{*\text{free}}/u_{h\text{free}}$, (ii) by using the WAsP recommended values and (iii) by using adjusted k_w values so that the IPW model matches the wind-speed reductions of the IWFBL model by Frandsen[9] for neutral conditions, a number of roughness values (as in Figure 7) and dimensionless turbine–turbine separations s. The models are evaluated with $h = 70$ m, $D_r = 80$ m, $A_* = 4.53$, $u_{h\text{free}} = 10$ m s^{-1} and latitude of 55.5°.

than for larger turbine separations and lower than the WAsP-k_w values for $z_o = 0.002$—0.02 m and $s < 10$. The lowest k_w values are given by the form $k_w = u_{*\text{free}}/u_{h\text{free}}$, which does not take the turbine separation into account.

In a similar fashion, a constant turbine to turbine distance, e.g., $s = 7$, can be used to analyze the behavior of the wind-speed reduction R_u for different atmospheric stability conditions and roughness lengths. This is illustrated in Figure 9. The wind-speed reductions for the IPW model using the form $k_w = u_{*free}/u_{h\text{free}}$ are generally higher than those for the extended IWFBL model by Frandsen, except for $z_o = 0.2$ m and a range of neutral to stable conditions. The results of the extended IWFBL model by Frandsen show an increase of R_u at a given positive h/L value because, as mentioned earlier, the reference wind speed is too high and MOST might be not longer valid. R_u does not vary with atmospheric stability in the IPW model as strongly (stability is accounted for through k_w only) as it does in the extended IWFBL model of Frandsen. The IPW model using the WAsP-k_w values shows similar reductions compared with those from the extended IWFBL model of Frandsen only for atmospheric conditions close to neutral.

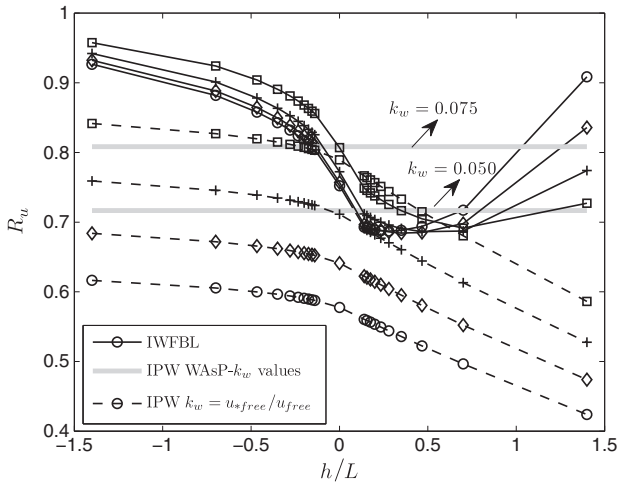

Figure 9. As in Figure 7 but for a range of dimensionless atmospheric stability conditions h/L and a constant dimensionless turbine–turbine separation $s = 7$. The models are evaluated with $h = 70$ m, $D_r = 80$ m, $u_{h\text{free}} = 10$ m s^{-1} and latitude of 55.5°.

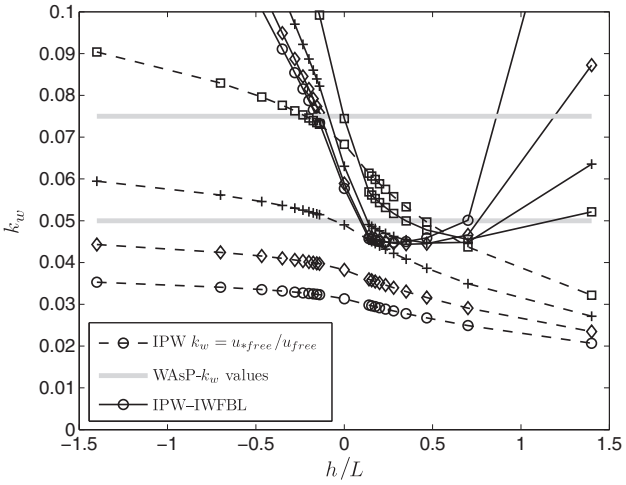

Figure 10. As in Figure 8 but for a range of dimensionless atmospheric stability conditions h/L and a constant dimensionless turbine–turbine separation $s = 7$. The models are evaluated with $h = 70$ m, $D_r = 80$ m, $u_{h\text{free}} = 10$ m s^{-1} and latitude of 55.5°.

The correspondent adjusted wake-decay coefficients, found when matching the wind-speed reduction of the IPW model to that of the extended IWFBL model of Frandsen for the different atmospheric stability conditions in Figure 9, are illustrated in Figure 10. The behavior of k_w with stability when assuming $k_w = u_{*\text{free}}/u_{h\text{free}}$ is similar to that found with the adjusted wake-decay coefficients for all roughness lengths, i.e., a decrease of the wake-decay coefficient the more stable the atmosphere, and generally shows the lowest k_w values (except when compared with the adjusted values for a narrow range of stable conditions and $z_o = 0.2$ m). The adjusted values tend to be much lower than the WAsP-recommended ones for a wide range of neutral to stable conditions and all roughness lengths. The increase of the adjusted k_w is due to the increase in R_u at the same stable h/L range, a behavior which disappears when the reference undisturbed wind speed is taken at a height within the surface boundary layer.

4. DISCUSSION

In this paper, k_w in the Park wake model for the infinite wind farm is, among others, adjusted so that the model matches the value of the wind-speed reduction of the extended IWFBL model of Frandsen. In a similar fashion, the adjustment can be performed using the IWFBL model of Emeis, which also shows that the WAsP-recommended values for k_w are generally

large for land-type roughness and short turbine separations. There are other WPW models, which use the k_w parameter, and here, we choose the Park wake model because it considers (among others) the effect of adjacent turbines, is a commonly used model and is the base of wind power calculations in WAsP. However, direct comparison and matching of the models are not totally fair because the wind-speed reduction estimated from the IWFBL models is related to the spatial average wind speed within the wind farm, whereas that from the IPW model is related to the wind speed immediately before the last turbine.

From our findings, we do not suggest to use the results for the wake-decay coefficient when performing wind power calculations directly, since the analysis is performed on the basis of the assumption either that $k_w = u_{*\text{free}}/u_{h\text{free}}$ or that of an infinite wind farm and in reality, only a couple of wind farms might be treated as such. For a finite but large wind farm, the first wake-affected turbines experience a rather different wake regime than those at the final rows perpendicular to the mean undisturbed wind direction and, therefore, k_w should be slightly decreased with downstream distance to values similar to ours under close turbine separations and near-stable conditions. An interesting and similar approach was shown by Rathmann *et al.*[26], in which after the k_w of the IPW model is adjusted to the IWFBL model of Frandsen, the WAsP-recommended k_w value in the Park model is gradually modified to asymptotically approach the infinite k_w value for 'deep' positions in the wind farm via a relaxation constant. Their approach agreed better than only assuming the WAsP-recommended values when compared with data from the Horns Rev and Nysted wind farms.

As wind turbines become larger, the IWFBL models have to be extended to account for effects that are normally not considered for small–medium turbines, which are well inside the surface boundary layer, such as the BLH. As illustrated in Figure 5, particularly for stable conditions, the wind speed predicted using MOST highly and sometimes unrealistically increases with height, and the addition of the BLH as a wind profile parameter will damp such unrealistic growth, as shown in the wind profile models by Peña *et al.*[10] over the sea, and Peña *et al.*[22] and Gryning *et al.*[27] over land. Unfortunately, from our knowledge, there is still a lack of BLH data for wind energy purposes, which can be used for model comparison.

Frandsen[28] attempted to compare theoretical wind-farm efficiencies by assuming that the change in roughness imposed by the infinite wind farm can be modeled as a smooth-to-rough generated internal boundary layer (IBL) to those derived from 'traditional' IBL models such as that of Miyake,[29] also used in WAsP for natural roughness transitions, finding similar results for an infinite row of turbines. However, as shown in Floors *et al.*,[30] although the IBL models give good results for neutral atmospheric conditions, observations of the IBL height show a strong dependency on atmospheric stability, which is normally neglected in the IBL models because it is generally believed that the mechanical contribution dominates the IBL growth. Since from our results the efficiency of the wind farm strongly depends on atmospheric stability, the question arises on how the IBL models can be adjusted for wind-farm efficiency analysis under different atmospheric conditions. Wind speeds within and downstream the wind farm are therefore needed to validate, for example, how accurate equation (20) describes the wind-farm characteristics by applying it to roughness models such as that in WAsP.

As previously mentioned, our results are difficult to compare with observations, since their analysis is at least as challenging as the modeling itself. Gaumond[16] found, for example, that the degree of accuracy of wake models evaluated for large offshore wind farms is much more dependent on the way data and simulations are post-processed than the physics of the models itself. There are, however, studies intending to reproduce the effects of large arrays of turbines on boundary layers by using LES techniques. Calaf *et al.*[14] 'immersed' medium-size and large-size arrays of turbines in a neutral boundary layer, and for all the different cases (varying the geometrical loading, aspect ratios s_r/s_f and roughness values), the LES-based average velocity profiles as stated in Calaf *et al.*[14] 'clearly showed the existence of two log laws above and below the turbine region', verifying the fundamental assumption of the IWFBL model of Frandsen. From their LES results, they proposed a new formulation of z_{oo} on the basis of that of Frandsen *et al.*[31] As their analysis of z_{oo}, our proposed expression in equation (20), is not very sensitive to the background roughness z_o but to atmospheric stability, which can be incorporated to those expressions in Calaf *et al.*,[14] and Meyers and Meneveau.[13] Lu and Porté-Agel,[12] on the other hand, studied an infinite large wind farm by horizontally applying periodic boundary conditions in a LES of the stable boundary layer covering a wind turbine. The shapes of their average velocity profiles are in good agreement with those in Calaf *et al.*,[14] and they found that the stable BLH considerably increased with simulation time, attributing this effect to radial and vertical wake expansions. We certainly believe that this is partly the case, but the BLH also increases because for all stability conditions, the above hub-height friction velocity, $\boldsymbol{u}_{*2}$, is higher than $u_{*\text{free}}$, which ends up lifting the BLH (in our model $\boldsymbol{u}_{*2}$ is about twice the value of $u_{*\text{free}}$ for stable conditions).

Here, we assume the local 'undisturbed' hub-height value of L to be representative of the upstream atmospheric stability conditions within the surface layer and higher (in cases where h is above it) and within the infinite wind farm. The local stability conditions inside wind farms actually vary because of the presence of the turbines, which change both the local momentum and buoyancy fluxes (L is related to the ratio between both) as Zhang *et al.*[32] showed from wind-tunnel experiments. Therefore, the vertical and horizontal stability homogeneity assumption does not probably hold, but this needs to be further investigated as there is a lack of experimental data to verify it. The models here presented predict the change of momentum flux, but there is no formulation for the buoyancy flux. Lu and Porté-Agel[12] showed that the presence of the turbines reduced the undisturbed surface friction velocity from 0.27 m s^{-1} to 0.23 m s^{-1} ($s = 8$) and 0.21 m s^{-1} ($s = 5$) (we find the same reductions for a wide range of roughness values, 0.0002 m $\ll z_o \ll$ 0.2 m, and neutral conditions), whereas

the undisturbed buoyancy flux (-4.3×10^{-4} m^2 s^{-3}) becomes -3.8×10^{-4} m^2 s^{-3} ($s = 8$) and -3.2×10^{-4} m^2 s^{-3} ($s = 8$). In terms of stability, this means a slight increase of instability from $L = 45$ m to $L = 32$ m and $L = 28$ m, respectively. Calaf *et al.*,[33] also using LES, found a scalar flux increasing within the wind farm by about 10–20%, which is in contrast with Zhang *et al.*'s reduction of the heat flux of 4% (in Zhang *et al.*,[32] the differences between the maximum and minimum heat fluxes are up to 12–7%).

5. CONCLUSIONS

The Park wake model has been used to derive the wind-speed reduction asymptotically reached by an infinite array of wind turbines and compared with the wind-speed reduction of the boundary-layer model of Frandsen for the infinite wind farm. The models show the same behavior for different dimensionless turbine to turbine separations and surface roughness lengths; the higher the roughness length and the longer the turbine separation, the lower the wind-speed reduction. The IPW model generally shows the highest wind-speed reductions, by assuming the form $k_w = u_{*\text{free}}/u_{h\text{free}}$ compared with those of the IWFBL model.

The IWFBL model of Frandsen has been extended to account for atmospheric static stability conditions (by assuming horizontal and vertical stability homogeneity) and shows a similar behavior with stability when compared with the IWFBL model of Emeis (the stability extended model of E&F); the more stable the atmosphere, the higher the wind-speed reduction, being the relative wind-speed reduction due to stability much higher than that due to surface roughness lengths (a wide range of roughness lengths has been considered). Emeis' model estimates lower wind-speed reductions than Frandsen's model for neutral conditions only and a wide range of wind speeds.

The extended IWFBL model of Frandsen shows that to get an increasing wind-speed reduction when going from neutral to stable conditions, it is required that the inputs to the model (i.e., the reference wind speed and atmospheric stability) are given close to the surface where MOST is fully valid. This results in a good estimation of the stability-corrected undisturbed friction velocity, which in turn provides a reasonable estimation of the geostrophic wind speed by using the stability-corrected A_* value.

The IWFBL model by Frandsen is the only one of the models here studied that is dependent on wind speed not only through the C_t curve of the turbine but also because it is geostrophic wind speed dependent. Thus, for a nearly constant C_t value, the wind-speed reduction increases anyway. However, at this stage, it is difficult to judge the quality of the models, since the IWFBL models, for example, either assume, among others, a relation between the mixing length and the height where the wind is undisturbed or a relation between the geostrophic and the hub-height wind-farm wind speed. Also, we do not validate the models against wind-farm data, but we expect to do so in the near future.

Finally, and most importantly, we are able to calibrate the 'more realistic' and more complex Park wake model to match the wind-speed reduction of the extended IWFBL model of Frandsen for different wind speeds, roughness values, turbine separations, turbine characteristics and atmospheric stability conditions by adjusting the value of the wake-decay coefficient, considering an infinite array of wind turbines. Already for neutral conditions, the k_w values are generally lower than those normally recommended by WAsP for wind power calculations for a number of surface roughness lengths and turbine separations lower than 10 rotor diameters. They are also strongly dependent on atmospheric stability, decreasing as the atmosphere becomes more stable, higher than the WAsP-recommended values for a number of roughness lengths under very unstable atmospheric conditions and much lower than those WAsP-recommended under neutral and a wide range of stable atmospheric conditions.

ACKNOWLEDGEMENTS

This work could not be possible without the lifetime work efforts of the late Sten T. Frandsen. Funding from the Danish Public Service Obligation (PSO) to the 'Windshadow' project, Energinet.dk 10086, and from the EERA-DTOC project is acknowledged. This work is performed in participation to the IEA-WakeBench research collaboration project. We would also like to thank Pierre-Elouan Réthoré and Søren Ott from DTU Wind Energy, Rebecca Barthelmie and the reviewers for the very useful comments on the manuscript.

APPENDIX A: SIMPLIFIED GEOSTROPHIC DRAG LAW DEPENDENCY ON ATMOSPHERIC STABILITY

The geostrophic drag law is given as

$$G = \frac{\boldsymbol{u}_*}{\kappa}\left(\left[\ln\left(\frac{\boldsymbol{u}_*}{f_c z_o}\right) - A(\mu_o)\right]^2 + B(\mu_o)^2\right)^{1/2}, \tag{24}$$

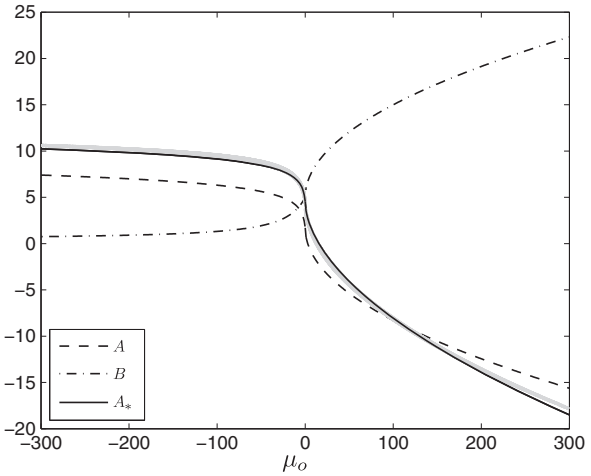

Figure 11. The dependency of the A, B and A_* parameters of the resistance laws on the dimensionless stability parameter μ_o. The gray points are the adjustment of A_* (equation (29)), to match the geostrophic wind from equation (24). The solid line corresponds to the forms $A_*(\mu_o \geq 0) = 4.53 - \mu_o^{0.55}$ and $A_*(\mu_o \leq 0) = 4.53 + \ln(1 - \mu_o)$.

where $A(\mu_o)$ and $B(\mu_o)$ depend on atmospheric stability since $\mu_o = \kappa \boldsymbol{u}_*/(f_c L)$.[19] Because of the scatter of the observations, there are numerous formulations for $A(\mu_o)$ and $B(\mu_o)$. We choose to use those of Jensen *et al.*[24] but with the values for neutral conditions ($\mu_o = 0$) adjusted to match the recent results of Peña *et al.*[22] and in consistency with the values used for the European Wind Atlas.[3]

$$A(\mu_o \geq 0) = 1.7 - \mu_o^{1/2}, \tag{25}$$

$$A(\mu_o \leq 0) = 1.7 + \ln(1 - \mu_o), \tag{26}$$

$$B(\mu_o \geq 0) = 5 + \mu_o^{1/2}, \tag{27}$$

$$B(\mu_o \leq 0) = \frac{5 - \kappa}{1 - \mu_o/25} + \kappa. \tag{28}$$

In the original formulation of Jensen *et al.*,[24] $\mu_o = u_*/(f_c L)$. However, we choose to include κ in μ_o, as in Zilitinkevich,[19] and Long and Guffey,[34] because the points used by Jensen *et al.*[24] to derive equations (25)–(27) were taken from the study of the Wangara data by Clarke and Hess,[35] where $\mu_o = \kappa \boldsymbol{u}_*/(f_c L)$.

For a range of dimensionless stabilities, G is computed from equation (24) by using the forms in equations (25)–(27). The result can then be used to estimate A_* from rearranging the simplified geostrophic drag law, in equation (4).

$$A_* = \ln\left(\frac{G}{f_c z_o}\right) - \frac{\kappa G}{\boldsymbol{u}_*}. \tag{29}$$

Figure 11 illustrates the results of such analysis, where an analytical form for $A_*(\mu_o)$ is also given.

APPENDIX B: EFFECTIVE WIND-FARM ROUGHNESS LENGTH

From equation (15), one can easily derive

$$\ln\left(\frac{z_{oo}}{h}\right) = -\frac{\kappa\, u_h}{u_{*2}} - \psi_m(h/L), \tag{30}$$

where the ratio $u_h/\boldsymbol{u}_{*2}$ can be replaced by $1/\sqrt{(\boldsymbol{u}_{*1}/u_h)^2 + c_t}$ from equation (1). Since $\boldsymbol{u}_{*1}/u_h = K_1^{-1}$, equation (30) then reads as

$$\ln\left(\frac{z_{oo}}{h}\right) = -\frac{\kappa}{\sqrt{c_t + K_1^{-2}}} - \psi_m(h/L), \tag{31}$$

from which z_{oo} can be derived (Frandsen *et al.*[31] deduced a similar form for neutral conditions only). It should be noted that the dependency on atmospheric stability of z_{oo} is through $\psi_m(h/L)$ and K_1, which also depends on $\psi_m(h/L)$.

APPENDIX C: THE INFINITE PARK WAKE MODEL

The total wake deficit $\delta_T = 1 - R_u$ of the Park wake model implemented in WAsP is estimated as the quadratic sum of four types of overlapping wakes:

$$\delta_T^2 = \delta_{\mathrm{I}}^2 + \delta_{\mathrm{II}}^2 + \delta_{\mathrm{III}}^2 + \delta_{\mathrm{IV}}^2. \tag{32}$$

The first term corresponds to the wakes directly upwind:

$$\delta_{\mathrm{I}}^2 = \delta_o^2 \sum_{j=1}^{\infty} d_w(s_j)^{-4} = \delta_o^2 \sum_{j=1}^{\infty} (1 + 2k_w s_r j)^{-4}, \tag{33}$$

where δ_o is the initial wake deficit, $\delta_o = \left(1 - \sqrt{1 - C_t}\right)$, d_w is a dimensionless wake diameter, $d_w = D_w/D_r$, with D_w as the wake diameter, $D_w = D_r(1 + 2k_w s_r)$, and j is the number of rows upwind from the considered turbine.

The second term corresponds to the reflected 'underground rotors' directly upwind:

$$\delta_{\mathrm{II}}^2 = \delta_o^2 \sum_{j=m_{\mathrm{II}}}^{\infty} d_w(s_j)^{-4} = \delta_o^2 \sum_{j=m_{\mathrm{II}}}^{\infty} (1 + 2k_w s_r j)^{-4}, \tag{34}$$

where m is the number of minimum rows to the first upwind row from where this type of wake has an effect on the considered turbine; in this case, $m_{\mathrm{II}} = (2h/D_r - 0.5)/(k_w s_r)$.

The third term corresponds to the shading rotors upwind but left or right to the wind direction:

$$\delta_{\mathrm{III}}^2 = \delta_o^2 \sum_{j=m_{\mathrm{III}}}^{\infty} 2N_{\mathrm{III}}(s_j) d_w(s_j)^{-4}, \tag{35}$$

where N_{III} is the number of turbines to the left and to the right of the wind direction that are able to throw their wake onto the considered turbine, $N_{\mathrm{III}}(s_j) = d_w(s_j)/(2s_f)$ and $m_{\mathrm{III}} = (s_f - 0.5)/(k_w s_r)$, so equation (35) becomes

$$\delta_{\mathrm{III}}^2 = \delta_o^2 \sum_{j=m_{\mathrm{III}}}^{\infty} \frac{d_w(s_j)}{s_f} d_w(s_j)^{-4} = \frac{\delta_o^2}{s_f} \sum_{j=m_{\mathrm{III}}}^{\infty} (1 + 2k_w s_r j)^{-3}. \tag{36}$$

The fourth term corresponds to the reflected shading 'underground rotors' upwind but left or right to the wind direction:

$$\delta_{\mathrm{IV}}^2 = \delta_o^2 \sum_{j=m_{\mathrm{IV}}}^{\infty} 2N_{\mathrm{IV}}(s_j) d_w(s_j)^{-4}, \tag{37}$$

where $N_{\mathrm{IV}}(s_j) = \sqrt{d_w(s_j)^2 - (4h/D_r)^2}/(2s_f)$ is the number of turbines to the left and to the right of the wind direction that are able to throw a reflected wake onto the considered turbine and $m_{\mathrm{IV}} = \left(\sqrt{s_f^2 + (2h/D_r)^2} - 0.5\right)/(k_w s_r)$, so equation (37) becomes

$$\delta_{\mathrm{IV}}^2 = \delta_o^2 \sum_{j=m_{\mathrm{IV}}}^{\infty} \frac{\sqrt{d_w(s_j)^2 - (4h/D_r)^2}}{s_f} d_w(s_j)^{-4} = \frac{\delta_o^2}{s_f} \sum_{j=m_{\mathrm{IV}}}^{\infty} \frac{\sqrt{(1 + 2k_w s_r j)^2 - (4h/D_r)^2}}{(1 + 2k_w s_r j)^4}. \tag{38}$$

The infinite sums converge and can be computed as

$$\delta_{\mathrm{I}}^2 = \frac{\delta_o^2 \ \mathrm{psi}\left[3, 1 + (2\, s_r\, k_w)^{-1}\right]}{96\, s_r^4\, k_w^4} \tag{39}$$

$$\approx \frac{\delta_o^2}{(1 + 2k_w s_r)^3}\left[\frac{1}{2(1 + 2k_w s_r)} + \frac{1}{6k_w s_r}\right], \tag{40}$$

$$\delta_{\mathrm{II}}^2 = \frac{0.0104167\, \delta_o^2 \ \mathrm{psi}\left[3, 2\, h/(s_r\, k_w)\right]}{s_r^4\, k_w^4} \tag{41}$$

$$\approx \frac{\delta_o^2}{128(h/D_r)^3}\left[\frac{1}{4(h/D_r)} + \frac{1}{3k_w s_r}\right] \tag{42}$$

$$\delta_{\mathrm{III}}^2 = \frac{-0.0625\, \delta_o^2 \ \mathrm{psi}\left[2, s_f/(s_r\, k_w)\right]}{s_f\, s_r^3\, k_w^3} \tag{43}$$

$$\approx \frac{\delta_o^2}{16 s_f^4}\left(1 + \frac{s_f/s_r}{k_w}\right), \quad \text{and} \tag{44}$$

$$\delta_{\mathrm{IV}}^2 \approx \frac{\delta_o^2}{16 s_f^4}\left[(1 + 4[(h/D_r)/s_f]^2)^{-2} + \left(\frac{s_f/s_r}{k_w}\right)\left(\frac{1 - [1 + 4([h/D_r]/s_f)^2]^{-3/2}}{6[(h/D_r)/s_f]^2}\right)\right]. \tag{45}$$

When using these last four results, one assumes that C_t is constant throughout the array, i.e., it does not strongly vary within the range of reduced wind speeds.

REFERENCES

1. Katic I, Højstrup J, Jensen NO. A simple model for cluster efficiency, *Proceedings of the European Wind Energy Association Conference & Exhibition*, 1986.
2. Mortensen NG, Heathfield DN, Myllerup L, Landberg L, Rathmann O. Getting started with WAsP 9. *Risø-I-2571(EN)*, Risø National Laboratory, Roskilde, *http:/www.wasp.dk/Download/DownloadFiles/General/Getting Started with WAsP 9.pdf*, 2007.
3. Troen I, Petersen EL. *European Wind Atlas*. Risø National Laboratory, Roskilde, 1989.
4. Peña A, Hahmann AN. Atmospheric stability and turbulent fluxes at Horns Rev—an intercomparison of sonic, bulk and WRF model data. *Wind Energy* 2012; **15**: 717–730.
5. Jensen LE. Array efficiency at Horns Rev and the effect of atmospheric stability, *Proceedings of the European Wind Energy Association Conference & Exhibition*, Milano, 2007.
6. Barthelmie R, Jensen LE. Evaluation of wind farm efficiency and wind turbine wakes at the Nysted offshore wind farm. *Wind Energy* 2010; **13**: 573–586.
7. Vincent CL, Pinson P, Giebel G. Wind fluctuations over the North Sea. *International Journal of Climatology* 2010. in press.
8. Sathe A, Gryning S-E, Peña A. Comparison of the atmospheric stability and wind profiles at two wind farm sites over a long marine fetch in the North Sea. *Wind Energy* 2011. in press.
9. Frandsen S. On the wind speed reduction in the center of large clusters of wind turbines. *Journal of Wind Engineering and Industrial Aerodynamics* 1992; **39**: 251–265.
10. Peña A, Gryning S-E, Hasager CB. Measurements and modelling of the wind speed profile in the marine atmospheric boundary layer. *Boundary-Layer Meteorology* 2008; **129**: 479–495.
11. Vermeer LJ, Sørensen JN, Crespo A. Wind turbine wake aerodynamics. *Progress in Aerospace Sciences* 2003; **39**: 467–510.
12. Lu H, Porté-Agel F. Large-eddy simulation of a very large wind farm in a stable atmospheric boundary layer. *Physics of Fluids* 2011; **23**: 065101 (1–19).
13. Meyers J, Meneveau C. Optimal turbine spacing in fully developed wind farm boundary layers. *Wind Energy* 2011. in press.

14. Calaf M, Meneveau C, Meyers J. Large eddy simulation study of fully developed wind-turbine array boundary layers. *Physics of Fluids* 2010; **22**: 015110 (1–16).
15. Emeis S, Frandsen S. Reduction of horizontal wind speed in a boundary layer with obstacles. *Boundary-Layer Meteorology* 1993; **64**: 297–305.
16. Gaumond M, Rethoré P-E, Ott S, Peña A, Bechmann A, Hansen KS. Evaluation of the wind direction uncertainty and its impact on wake modelling at the Horns Rev offshore wind farm. *Wind Energy* 2013. in press.
17. Jensen NO. Change of surface roughness and the planetary boundary layer. *Quarterly Journal of the Royal Meteorological Society* 1978; **104**: 351–356.
18. Rethoré P-E. Wind turbine wake in atmospheric turbulence. *Technical Report Risoe-PhD-53(EN)*, Risø DTU, Roskilde, 2009.
19. Zilitinkevich SS. Resistance laws and prediction equations for the depth of the planetary boundary layer. *Journal of Atmospheric Sciences* 1975; **32**: 741–752.
20. Emeis S. A simple analytical wind park model considering atmospheric stability. *Wind Energy* 2010; **13**: 459–469.
21. Monin AS, Obukhov AM. Osnovnye zakonomernosti turbulentnogo peremeshivanija v prizemnom sloe atmosfery (basic laws of turbulent mixing in the atmosphere near the ground). *Trudy Geofizicheskogo Instituta AN SSSR* 1954; **24**(151): 163–187.
22. Peña A, Gryning S-E, Hasager CB. Comparing mixing-length models of the diabatic wind profile over homogeneous terrain. *Theoretical and Applied Climatology* 2010; **100**: 325–335.
23. Peña A, Gryning S-E, Mann J. On the length-scale of the wind profile. *Quarterly Journal of the Royal Meteorological Society* 2010; **136**: 2119–2131.
24. Jensen NO, Petersen EL, Troen I. Extrapolation of mean wind statistics with special regard to wind energy applications. *Technical Report WCP–86, WMO/TF–No. 15*, World Meteorological Organization, 1984.
25. Jensen NO. A note on wind generator interaction. *Technical Report Risoe-M-2411(EN)*, Risø National Laboratory, Roskilde, 1983.
26. Rathmann OS, Frandsen S, Nielsen M. Wake decay constant for the infinite wind turbine array, *Proceedings of the European Wind Energy Association Conference & Exhibition*, Warsaw, 2010.
27. Gryning S-E, Batchvarova E, Brümmer B, Jørgensen H, Larsen S. On the extension of the wind profile over homogeneous terrain beyond the surface layer. *Boundary-Layer Meteorology* 2007; **124**: 251–268.
28. Frandsen ST. Turbulence and turbulence-generated structural loading in wind turbine clusters. *Technical Report Risoe-R-1188(EN)*, Risø DTU, Roskilde, 2007.
29. Miyake M. Transformation of the atmospheric boundary layer over inhomogeneous surfaces. *Technical Report Unpublished MSc. Thesis, Science Report 5R-6*, University of Washington, Seattle, 1965.
30. Floors R, Gryning S-E, Peña A, Batchvarova E. Analysis of diabatic flow modification in the internal boundary layer. *Meteorologische Zeitschrift* 2011; **20**: 649–659.
31. Frandsen S, Barthelmie R, Pryor S, Rathmann O, Larsen S, Højstrup J, Thøgersen M. Analytical modelling of wind speed deficit in large offshore wind farms. *Wind Energy* 2006; **9**: 39–53.
32. Zhang W, Markfort CD, Porté-Agel F. Experimental study of the impact of large-scale wind farms on land-atmosphere exchanges. *Environmental Research Letters* 2013; **8**: 015002 (8 pp).
33. Calaf M, Parlange MB, Meneveau C. Large eddy simulation study of scalar transport in fully developed wind-turbine array boundary layers. *Physics of Fluids* 2010; **23**: 126603 (1–16).
34. Long RR, Guffey LJ. Drag and heat transfer relations for the planetary boundary layer. *Boundary-Layer Meteorology* 1977; **11**: 363–373.
35. Clarke RH, Hess GD. Geostrophic departure and the functions a and b of rossby-number similarity theory. *Boundary-Layer Meteorology* 1974; **7**: 267–287.